EVALUATION OF THE USEFULNESS OF TEXTURE MEASURES FOR CROP TYPE CLASSIFICATION BY HYPERION DATA

H.ASHOORI [a*], H. FAHIMNEJAD[b], A. ALIMOHAMMADI[c], S.R. SOOFBAF[d]

Geodesy and Geomatic Faculty, K.N.Toosi University of Technology, Tehran, Iran -
[a] Hamed_Ashoori@yahoo.om, [b]hamed_fahimnejad@yahoo.com, [c]alimoh_abb@yahoo.com, [d]sr.soofbaf@gmail.com

Commission VIII, WG VIII/10

KEY WORDS: Hyperspectral, Texture Quantization, Classification, Hyperion, Linear Spectral Unmixing

ABSTRACT:

Availability of new generation of hyperspectral sensors such as the Hyperion has lead to new challenges in the area of crop type mapping and agricultural management. Many crops like wheat and barley are spectrally similar and may not be discriminated by the normally available multispectral data. Although the existing hyperspectral data provide the possibilities for discrimination of crop types, but consideration of spatial variability between the adjacent pixels known as the texture data, can lead to more accurate results in a classification process. In this research, Hyperion data of an agricultural area located in south of Tehran, has been examined for discrimination of wheat and barley fields. The output bands of linear unmixing algorithm have been used as inputs for texture feature generation by different methods including the First Order Statistics of the Gray Level Co-occurrence Matrix, Geostatistics and Fourier Transform. Maximum likelihood classifier has been applied to classify the different combinations of linear unmixing outputs and texture features. Overall accuracies as well as the producer accuracies have been used as the evaluation criteria for different classifications. Results of this work have shown that the use of texture features generated from the output bands of linear unmixing algorithm lead to higher accuracies. Overall accuracy improved up to 7% and better discrimination between similar classes where obtained.

1. INTRODUCTION

1.1 Overview

The Hyperion sensor onboard NASA's Earth Observing 1 (EO-1) satellite is the first spaceborne hyperspectral instrument to acquire both visible/near-infrared (400-1000 nm) and shortwave infrared (900-2500 nm) spectral data (Pearlman, 2003). Because of having 242 potential bands and spatial resolution of 30 m, the sensor bears potentials to provide data for both detailed land use classification and estimation of biogeophysical and chemical properties of heterogeneously vegetated areas.

In this study, usefulness of texture quantization methods for improving discrimination of crop types has been investigated.

1.2 The study Site

An agricultural area located in southern parts of Tehran, known as Ahmadabad has been selected as the study site. Wheat and barley are the main agricultural crops in the area. More than 30 fields of detailed ground-truth dataset have been visited in the field and their records have been used as a reference data for training and verifying the results of the classification.

1.3 Hyperspectral Data

Hyperion data were acquired over the study area on May 21, 2002 at 06:57:56 GMT. The EO-1 satellite is a sun-synchronous orbit at 705 km altitude. Hyperion data includes 256 pixels with a nominal size of 30 m on the ground over a 7.65 km swath. Well-calibrated data (Level 1B1) is normally available. Hyperion data is acquired in pushbroom mode with two spectrometers. One operates in the VNIR range (including 70 bands between 356-1058 nm with an average FWHM of 10.90 nm) and the other in the SWIR range (including 172 bands between 852- 2577nm, with an average FWHM of 10.14 nm). 44 of 242 bands including bands 1-7, 58-76 and 225-242 are set to zero by TRW software during Level 1B1 processing (Pearlman, 2003).

2. REMOTE SENSING DATA PREPARATION

Post-level 1B1 data processing operations for Hyperion data included band selection (Datt, et al, 2003), correction for bad lines (Han, et al., 2002), striping pixels (Datt, et al, 2003) and smile (Goodenough, et al, 2003), a pixel-based atmospheric correction using FLAASH (Beck R et al., 2003) and a co-alignment. A brief explanation of these is provided as follow.

2.1 Band selection

Atmospheric water vapor bands which absorb almost the entire incident and reflected solar radiation and the bands that have very severe vertical stripping are usually identified by visual inspection of the image data or atmospheric modeling (Beck R et al., 2003). The subset of 160 selected bands are listed in Table I.

Array	Bands	Wavelength(nm)
VNIR	8 t0 57	427 to 926
SWIR	83 to 119	973 to 1336
	130 to 164	1447 to 1790
	181 to 184	1962 to 1992
	187 to 220	2022 to 2355

Table 1. List of the selected 160 bands used for this research

2.2 Bad line correction

Bad lines in Hyperion level 1B1 data appear as dark vertical lines. These pixels have lower DN values as compared to their neighboring pixels. These pixels were corrected by replacing their DN values with the average DN values of their immediate left and right neighboring pixels (Han, et al., 2002).

2.3 Correction of striping Pixels

Vertical stripes are caused by differences in gain and offset of different detectors in pushbroom-based sensors. Statistics of the detector arrays can be studied by accumulating mean, variance, minimum, and maximum data for each pixel in each band over the lines of an image. As discussed above, Vertical stripe occurs where the statistics indicates, that the image information is valid (that is not considered as bad pixel) but with significantly modified gain and offset. It is assumed that such gains and offsets are relatively stable over a collect but not necessarily between collects (Beck et al., 2003).

A general approach for removing vertical stripes with these characteristics is similar to methods used in the past to balance horizontal stripes in mirror scanner images by histogram equalization or to flatten images affected by limb brightening or to balance detectors in airborne pushbroom sensors (Beck et al., 2003). That is, histogram moments, such as the means and variances of the columns in each band, are used to balance the statistics of the arrays to those of a reference histogram.

The pixel balancing applied here is different in that it may be used either "globally" or "locally." In global balancing, the statistical moments of each column are modified to match those for the whole image for each band. In the local approach, reference moments are estimated locally (Beck et al., 2003). In this research, global balancing method was used.

2.4 Smile Correction

Smile, which exists in all Hyperion datasets, refers to an across-track wavelength shift from the center wavelength, which is due to the change of dispersion angle with field position.

According to the Hyperion spectral calibration (Goodenough, et al., 2003), the shifts are dependent on pixel position in the across-track direction. For VNIR bands, the shifts range between 2.6–3.5nm. For SWIR bands, the shifts are less than 1 nm and are not significant for agricultural applications (Goodenough, et al., 2003). Considering the high spectral resolution of the Hyperion data, the 2.6–3.6-nm shifts of VNIR bands cannot be ignored, in this case the pixel spectra may result in reduction of classification accuracies. Column Mean Adjustment in Radiance Space method was used for smile correction in this research (Goodenough, et al., 2003).

2.5 Co-alignment

A shift of one pixel in the line direction was corrected in the SWIR image data. This shift occurred between pixel positions 128 and 129. A spatial misregistration between the VNIR and SWIR data was detected. A co-alignment between the two datasets is achieved by a counter-clockwise rotation followed by a negative one-pixel shift in the line direction.

These operations were carried out on the VNIR data, which were then resampled with a piecewise linear interpolation based on the values of the nearest eight points. The VNIR were matched to the SWIR data. The co-alignment was carried out prior to atmospheric correction in order to use the 940-nm water vapour absorption in combination with the one located at 1130-nm for scene-based retrieval of water vapour content on a pixel basis (Staenz, et al., 2002).

2.6 Atmospheric Correction

Atmospheric correction of the 160 channels of Hyperion dataset was performed by using FLAASH, an atmospheric correction program based on look-up tables generated with a radiative transfer code (MODTRAN-4) (FLAASH Module User's Guide., 2005).

3. ENDMEMBER AND FEATURE EXTRACTION

In conventional information extraction from hyperspectral images, endmembers as a reference data for classification process should be specified. They may be obtained from a spectral library, spectrometric measurement or be extracted from the image.

Commonly used classification algorithms include unmixing methods (FAHIMNEJAD, et al., 2007). But an important limitation of unmixing for crop type classification is the problem of threshold determination. Classification of unmixing results and texture data as implemented in this research, overcomes this limitation,

3.1.Endmember extraction

Theoretically the existing pure features in mixed pixels are refered to as endmembers. Selection and identification of spectral endmembers in an image is the key point to success of the linear spectral mixing model. Collection of endmembers should allow the description of all spectral variability for all pixels.

Endmembers resulting from the use of the existing library of reflectance spectra are denoted as known endmembers. Whereas extraction of the purest pixels from the image data itself results in the derived endmembers. Because of the lack of access to spectral library or field measurements of spectral properties of land cover types of interest, endmember data of the known ground cover types were extracted from the Hyperion data. Three endmembers including soil, wheat and barley crops as extracted from the Hyperion data are represented in figure 1.

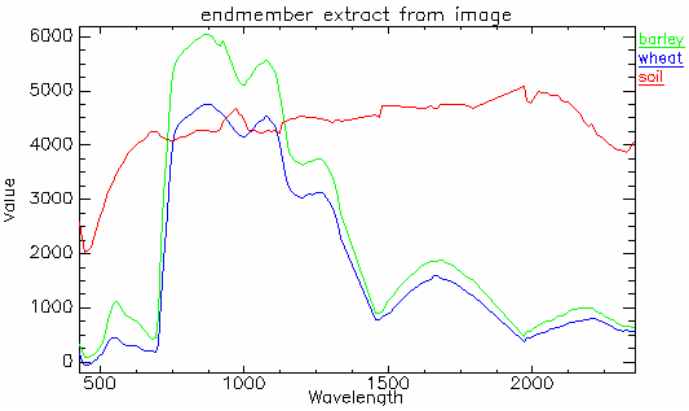

Figure 1: Spectral profile of 3 endmembers extracted from the Hyperion Data

3.2.Linear Spectral Unmixing

A simple and commonly used method of mixture analysis is the linear model. In this model, the spectrum is considered as a linear combination of the "pure" spectra of the materials located in the pixel area, weighted by their fractional abundance (Shresthad, et al., 2002). In linear mixture modeling the resulting pixel reflectance spectrum is assumed to be a summation of the individual material reflectance functions multiplied by their fraction. That means with known number of endmembers and by having the spectra of each pure component, the observed pixel value in any spectral band can be modeled by the linear combination of the spectral response of components within the pixel. The linear mixture model for a pixel, with the observed reflectance r_i in band i can be described as:

$$r_i = \sum_{j=1}^{n} f_j a_{ij} + \varepsilon_i \quad (1)$$

Where n is the number of endmembers

f_j : Fraction of endmember j

a_{ij} : Spectral response of Endmember j in band i

ε_i : Error term

Using these techniques it is possible to derive the relative or absolute abundance of a number of spectrally pure components, together termed as endmembers, contributing to the observed reflectance of the pixel. Therefore, the fractions at each pixel (the unmixing result) can be computed by taking the inverse of equation 2.

Additionally, one can impose constraints upon the solutions of equation 2. One set of constraints requires the fractions within a pixel to sum to unity.

$$\sum_{i=1}^{n} f_i = 1 \quad (2)$$

A fully constrained set would also require that each individual fraction to lie between 0 and 1:

$$0 \le f_i \le 1 \quad (3)$$

For the purpose of crop type discrimination, results of the linear spectral unmixing were classified based on commonly used methods. Then linear unmixing output bands, were used as input bands for different texture quantization methods, and generated features together with the linear unmixing bands were used for classification.

3.3.Texture Feature Generation

The result of linear unmixing includes three bands, which are the proportions of existence of three main classes (wheat, barley and soil) in a pixel.

Texture classification is a known method to classify high resolution images; also it can be used to generate extra features to use as input data for classification methods (Ashoori, et al., 2006).

There are different methods for quantifying texture, in this paper several methods were used to generate features from three available features. First order Statistical, Gray level Co-Occurrence matrix based, Geostatistical, Fourier Transform and Wavelet based methods were used to generate new texture features.

These are briefly described below :

3.3.1 First Order Statistical Features: If (I) is the random variable representing the gray levels in the region of interest, the first order histogram P (I) is defined as (Theodoridis, 1999):

$$P(I) = \frac{number\ \ of\ \ pixels\ \ whith\ \ gray\ \ level\ \ I}{Total\ \ number\ \ of\ \ pixels} \quad (4)$$

Now different features can be generated by using the following equations:

3.3.2. Moment

$$m_i = E\left[I^i\right] = \sum_{I=0}^{N_g-1} I^i P(I) \qquad i = 1,2,3,.... \quad (5)$$

Where N_g = number of gray levels.

$m_1 = E[I]$ is the simple mean of pixels. Also 2nd, 3rd and other moments can be used.

3.3.3.Central Moments

$$\mu_i = E\left[(I - E[I])^i\right] = \sum_{I=0}^{N_g-1} (I - m_1)^i P(I) \quad (6)$$

3.3.4.Absolute Moments

$$\hat{\mu}_i = E\left[Abs(I - E[I])^i\right] \quad (7)$$

3.3.5.Entropy

$$H = -E\left[\log_2 P(I)\right] = -\sum_{I=0}^{N_g-1} P(I) \log_2 P(I) \quad (8)$$

3.3.6.Median: Median is the middle value in a set of numbers arranged in increasing order. Because the kernel size always

covers odd number of pixels, median can be extracted simply by choosing the mid member of an array which contains gray levels of pixels that covered by the mask and then it is sorted.

3.3.7.Mode: Mode is the most frequent value of a random variable. So in an image mode is the most frequent pixel gray level.

3.3.8.Distance Weighted Mean: If the distance from center pixel is considered as the weight for computing the mean then near pixels have more contribution in the results.

$$Mean_w = \frac{\sum_{i=1}^{N_r}\sum_{j=1}^{N_c}\frac{1}{d_{i,j}}I(i,j)}{\sum_{i=1}^{N_r}\sum_{j=1}^{N_c}\frac{1}{d_{i,j}}} \quad (9)$$

3.3.9.Gray level Co-Occurrence Based Features: Haralick et.al proposed this method to extract texture information from digital images. First Gray level co-occurrence matrix (GLCM) is produced and then several texture measures are computed from it. GLCM is a matrix that contains the number of each gray level pairs that are located at distance d and direction θ from each other. This matrix can be defined for different distances, angles and as well as for different lags.

$$GLCM_{d_i,d_j} = \frac{1}{R}\begin{bmatrix} \eta(0,0) & \eta(0,1) & . & . & \eta(0,N_{g-1}) \\ \eta(1,0) & \eta(1,1) & . & . & . \\ . & . & . & \eta(i,j) & . \\ . & . & . & . & . \\ \eta(N_{g-1},0) & . & . & . & \eta(N_{g-1},N_{g-1}) \end{bmatrix}$$

$\eta(i,j)$ #Pixel Pairs in lag (d_1,d_2) through

N_g : Number of Gray Levels

R : Total Number of Possible Pairs (10)

In this research, following features have been generarted from the GLCM matrix :

3.3.10.Mean

$$\mu_i = \sum_{i=0}^{N_{g-1}}\sum_{j=0}^{N_{g-1}} i \times P(i,j) \quad \mu_j = \sum_{i=0}^{N_{g-1}}\sum_{j=0}^{N_{g-1}} j \times P(i,j) \quad (11,12)$$

where P(i,j)=GLCM(i,j)

3.3.11.Variance

$$\sigma_i^2 = \sum_{i=0}^{N_{g-1}}\sum_{j=0}^{N_{g-1}} (i-\mu_i)^2 \times P(i,j) \quad (13)$$

$$\sigma_j^2 = \sum_{i=0}^{N_{g-1}}\sum_{j=0}^{N_{g-1}} (j-\mu_i)^2 \times P(i,j) \quad (14)$$

Mean and variance of GLCM are not the same as for the image because the frequency of occurrence of different pairs is modeled here.

3.3.12.Homogeneity (Inverse Differences Moment)

$$IDF = \sum_{i=0}^{N_{g-1}}\sum_{j=0}^{N_{g-1}} \frac{P(i,j)}{1+(i-j)^2} \quad (15)$$

It assigns higher weight to the main diagonal of GLCM so it produces higher values for images that have larger homogeneous areas.

3.3.13.Contrast

$$CON = \sum_{i=0}^{N_{g-1}}\sum_{j=0}^{N_{g-1}} (i-j)^2 P(i,j) \quad (16)$$

The more the distance from the main diagonal of GLCM the higher the weight that is assigned to the P(i,j), so when the difference between neighboring pairs becomes large, the contrast increases.

3.3.14.Dissimilarity

$$CON = \sum_{i=0}^{N_{g-1}}\sum_{j=0}^{N_{g-1}} |i-j| P(i,j) \quad (17)$$

It works like contrast but gives lower weight to the difference of each gray level pairs.

3.3.15.Entropy

$$Entropy = -\sum_{i=0}^{N_{g-1}}\sum_{j=0}^{N_{g-1}} P(i,j)\ln(P(i,j)) \quad (18)$$

It outputs higher value for a homogeneous distribution of P(i,j), and lower otherwise.

3.3.16.Angular Second Moment

$$ASM = \sum_{i=0}^{N_{g-1}}\sum_{j=0}^{N_{g-1}} \left(P(i,j)\right)^2 \quad (19)$$

It is a measure of image smoothness. It outputs higher values when P(i,j) is concentrated in a few places in the GLCM and lower if the P(i,j) are close in value.

3.3.17.Correlation

$$Correlation = \sum_{i=0}^{N_{g-1}} \sum_{j=0}^{N_{g-1}} \frac{(i-\mu_i)(j-\mu_j)P(i,j)}{\sigma_i \sigma_j} \quad (20)$$

It measures linear dependency of gray levels on those of neighboring pixels.

3.3.18.Geostatistical Features: Geostatistics is the statistical methods developed for and applied to geographical data. These statistical methods are required because geographical data do not usually conform to the requirements of standard statistical procedures, due to spatial autocorrelation and other problems associated with spatial data (http://www.geo.ed.ac.uk).

Semivariogram that represents half of the expectation of the quadratic increments of pixel pair values at the specified distance can quantify both spatial and random correlation between the adjacent pixels. (Goodenough, et al, 2003) It is defined as:

$$\gamma(h) = \frac{1}{2n(h)} \sum_{i=1}^{N_r - h_1} \sum_{j=1}^{N_c - h_2} [DN(i,j) - DN(i+h_1, j+h_2)]^2 \quad (21)$$

That is the classical expression of variogram (h) here represents a vectorial lag between pixels. In this study direct variogram, madogram, cross variogram and pseudo-cross variogram have been used. The first two operate separately for each image bands and the second two operate for pairs of image bands.

3.3.19.Direct Variogram : In this approach the following equation is used to estimate:

$$\gamma(h) = \frac{1}{2n(h)} \sum_{i=1}^{N_r - h_1} \sum_{j=1}^{N_c - h_2} (DN(i,j) - DN(i+h_1, j+h_2))^2 \quad (22)$$

n(h) is the number of pairs that are in mask filter.

3.3.20.Madogram: This is similar to direct variogram except that squaring differences, are replaced by the absolute values of differences.

$$\gamma(h) = \frac{1}{2n(h)} \sum_{i=1}^{N_r - h_1} \sum_{j=1}^{N_c - h_2} \left| DN(i,j) - DN(i+h_1, j+h_2) \right| \quad (23)$$

3.3.21.Cross Variogram: Two image bands are used to quantify the joint spatial variability between bands.

$$\gamma_{m,n}(h) = \frac{1}{2n(h)} \sum_{i=1}^{N_r - h_1} \sum_{j=1}^{N_c - h_2} \{[DN_m(i,j) - DN_m(i+h_1, j+h_2)] * \left[DN_n(i,j) - DN_n(i+h_1, j+h_2)\right]\} \quad (24)$$

3.3.22.Pseudo-cross Variogram: It is similar to direct variogram, but uses pairs which are from two different bands (m,n).

$$\gamma_{m,n}(h) = \frac{1}{2n(h)} \sum_{i=1}^{N_r - h_1} \sum_{j=1}^{N_c - h_2} [DN_m(i,j) - DN_n(i+h_1, j+h_2)]^2 \quad (25)$$

3.3.22.Fourier Based Features: Fourier transformation, transforms a signal from space/time domain to frequency domain. The amplitude and phase coefficients are two outputs of a Fourier transformation. So different texture patterns could be identified by their Fourier coefficients but because in this research one value for each pixel is required, raw Fourier coefficients couldn't be used. Several features can be generated using sum of the Fourier amplitude under different masks (Pratt, 2001). These include ringing, sectorial, horizontal and vertical which are shown in figure 2.

$$F(u,v) = \frac{1}{N} \sum_{x=0}^{N-1} \sum_{y=0}^{N-1} f(x,y) e^{-j\frac{2\pi}{N}(ux+vy)} \quad (26)$$

$$FourierAmplitude: A(u,v) = \left| F(u,v) \right|^2$$

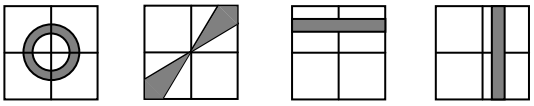

Figure2. Different mask which can be used to generate features from Fourier coefficients

P(i,j) is the (i,j)th pixel of approximation band of wavelet transformed image in specific level.

First and second levels of wavelet transformation were used.

Different parameters can be set in each method, the main parameter is window size. Different window sizes from 3 to 15 were used to generate features in each method.

4. CLASSIFICATION

Linear unmixing outputs were used as input bands for texture generation. Then maximum likelihood supervised classification was used to classify different combinations of those three linear unmixing output bands and textures features generated from different methods, with different window sizes and different distance vector in GLCM and Geostatistics and different masks in the fourier method.

177 pixels were defined as training data and 3850 pixels were used as check data to evaluate the classification accuracy. These data were collected through filed work.

Producer accuracy for each class, overall accuracy and kappa coefficient were calculated for each combination to evaluate each method.

5. RESULTS AND CONCLUTION

As compared to results obtained by thresholding of unmixing outputs which needs field work to specify the thresholds (Fahimneszhad, et al., 2007) higher overall accuracies has been obtained, by the use of texture data which is mainly based on the most commonly used maximum likelihood classifier. The improvement of accuracy is up to 7% in overall accuracy and up to 20% in producer accuracies. These results show that using

texture features has resulted in better discrimination of the similar classes.

Some of interesting results of this research together with the resulting classification are shown in table 2 and figure 3. Classification of figure 3 has been identified as the most correct classification and has been obtained from classification of the three linear unmixing outputs and the corresponding pseudo-cross variogram features.

Accuracy of classifications resulting from different features show high differences with Geostatistics showing the best performance. Other methods in order of performance include First Order Statistic, Gray Level Co-Occurance Matrix and the fourier based features.

As a general rule, features which are generated by using larger kernel sizes don't lead to higher accuracies. Because, larger kernels act very similar to low pass filters and may ignore the local and high frequency details.

Method (the number shows the generated feature)	Distance Vector	Kernel Size	Wheat P.A.	Barley P.A.	Soil P.A.	Overall	Kappa
Geostatistics(4)	1,1	3	96.6	92.82	100	95.25	0.92
GLCM (7)	0,1	3	93.59	94.97	100	95.07	0.92
GLCM (6)	1,1	5	93.99	93.45	100	94.51	0.91
First Statistic (3)	-	9	98.2	89.04	100	94.11	0.9
Geostatistics(4)	1,0	3	96.46	90.62	99.38	94.08	0.9
GLCM (7)	1,1	5	95.13	91.13	100	93.87	0.9
Geostatistics(4)	1,-1	3	96.26	90.23	99.17	93.79	0.9
Geostatistics(4)	0,1	3	97.66	88.42	99.79	93.58	0.89
Geostatistics(4)	1,1	5	96.8	89.32	98.96	93.55	0.89
GLCM-16(6)	1,0	5	94.93	89.77	100	93.15	0.89
First Statistic (3)	-	5	99.67	84.75	100	92.67	0.88
First Statistic (2)	-	5	94.93	88.19	100	92.4	0.87
GLCM 6)	1,-1	5	95.66	87.34	100	92.3	0.87
GLCM (7)	1,-1	5	92.59	89.66	100	92.16	0.87
GLCM (3)	0,1	5	96.53	86.27	100	92.14	0.87
GLCM (10)	1,1	7	91.19	90.56	100	92.03	0.87
GLCM (7)	1,0	5	95.46	86.72	100	91.92	0.87
GLCM (3)	1,0	5	95.86	86.33	100	91.9	0.87
Geostatistics(4)	1,0	5	95.93	86.27	98.96	91.76	0.86
Geostatistics(All)	All	3	94.99	87.29	97.1	91.63	0.86

Table 2. Overall accuracy of the best 20 classification resulting from the integrated use of texture data

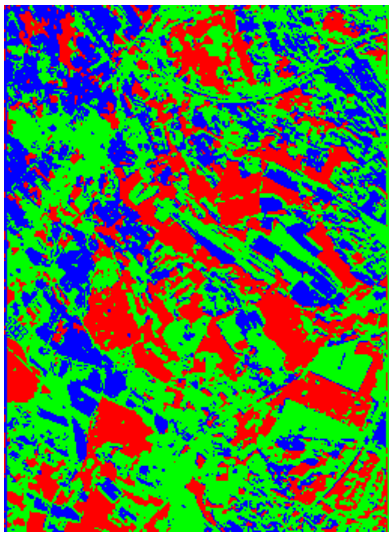

Figure3. Classified image resulting from classification of unmixing and texture data (Red: Soil, Green: Barley, Blue: Wheat)

REFERENCES

References from Journals:

Chica-Olmo,M., Abarca-HernaÂndez,F.,2000. Computing geostatistical image texture for remotely sensed data classification, Computers & Geosciences 26 ,pp 373-383.

Datt, B., McVicar, T.R., Van Niel, T.G., Jupp, D.L.B., and Pearlman, J.S., 2003. Preprocessing EO-1 Hyperion Hyperspectral Data to Support the Application of Agricultural Indexes. *IEEE Trans. Geosci. Remote Sensing*, 41(2), pp.1246-1259.

Goodenough, D.G., Dyk, A., Niemann, O., Pearlman, J.S., Chen, H., Han, T., Murdoch, M., and West, C., 2003.Processing HYPERION and ALI for Forest Classification.IEEE Trans. Geosci. Remote Sensing, 41(2), pp.1321-1331.

Haralick, R.M., Shanmugam, K., Dinstein, I., 1973. Textural features for image classification. IEEE Transactions on Systems, Man and Cybernetics, vol. 3, no. 6, pp 610-621.

Staenz, K., Neville R.A., H.P. and White, S., 2002. Retrieval Of Surface Reflectance From Hyperion Radiance Data, IEEE International Geoscience and Remote Sensing Symposium.

References from Books:

Castleman, K.R., 1996. Digital Image Processing. Prentice-Hall.

Chain-I, Chang, 2003. Hyperspectral imaging: techniques for spectral detection and classification, Kluwer academic/plenum Publisher, Newyork, N.Y.

Pratt, 2001. Digital Image Processing, JOHN WILEY & SONS.

Theodoridis, S., 1999. Pattern Recognition. Academic Press.

References from Other Literature:

Ashoori, H., Alimohammadi, A., Valadan Zoej, M. J., Mojarradi, B., 2006. Generating Image-based Features for Improving Classification Accuracy of High Resolution Images, May, ISPRS Mid-term Symposium, Netherlands.

Beck R, 2003. EO-1 User Guide v. 2.3. Department of Geography University of Cincinnati.

Fahimnejad, H., Soofbaf, S.R., Alimohammadi, A., Valadan Zoej, M. J., 2007. Crop types classification by Hyperion data and unmixing algorithm",MapWorldForum.

FLAASH Module User's Guide, ENVI FLAASH Version 4.2 August, 2005 Edition.

Han, T., Goodenough, D. G., Dyk, A., and Love, J. 2002. Detection and correction of abnormal pixels in Hyperion image. IGARSS, vol. III, Toronto, ON, Canada, pp. 1327–1330.

Pearlman J.S., 2003. Hyperion Validation Report. Boeing Report Number 03-ANCOS-001.

Shresthad, D.P., Margate, D.E., Anh, H.V. and Van Der Meer, F., 2002. Spectral unmixing versus spectral angle mapper for land degradation assessment: a case study in Southern Spain. 17th WCSS, 12-21 August,Thailand,Symposium no.52.

References from websites:
http://www.geo.ed.ac.uk (accessed 10 Jan. 2002)